HHS Public Access

Author manuscript

J Colloid Interface Sci. Author manuscript; available in PMC 2020 April 15.

Published in final edited form as:

J Colloid Interface Sci. 2019 April 15; 542: 370–378. doi:10.1016/j.jcis.2019.02.021.

Ultrafast microfluidic synthesis of hierarchical triangular silver core-silica shell nanoplatelet toward enhanced cellular internalization

Nanjing Hao, **Yuan Nie**, **Zhe Xu**, and **John X.J. Zhang***

Thayer School of Engineering, Dartmouth College, 14 Engineering Drive, Hanover, New Hampshire 03755, United States.

Abstract

Microfluidic reactors represent a new frontier in the rational design and controllable synthesis of functional micro-/nanomaterials. Herein, we develop a continuous and ultrafast flow synthesis method to obtain triangular silver (tAg) nanoplatelet using a short range two-loop spiral-shaped laminar flow microfluidic reactor, with one inlet flow containing $AgNO_3$, trisodium citrate, and H_2O_2 and the other $NaBH_4$. The effect of the reactant concentration and flow rate on the structural changes of tAg is examined. Through the same miniaturized microreactor, hierarchical core-shell $Ag@SiO_2$ can be produced with tunable silica shell thickness using one inlet flow containing the as-synthesized Ag nanoparticles together with tetraethyl orthosilicate and the other ammonia. The enhanced cellular internalization efficiency of triangular nanoplatelets by PANC-1 and MCF-7 cells is further confirmed in comparison with the spherical ones. These results not only bring new insights for engineering nanomaterials from microreactors but also facilitate the rational design of functional nanostructures for enhancing their biological performance.

Graphical Abstract

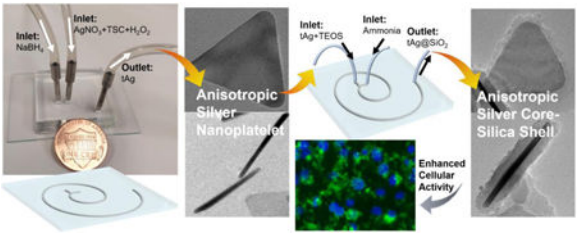

Keywords

Microfluidics; Hierarchical; Core-shell; Nanoplatelet; Cellular internalization

* john.zhang@dartmouth.edu.

1. Introduction

Anisotropic nonspherical micro-/nanomaterials have attracted extensive interests due to their superior physicochemical and biological properties in diverse fields over their spherical counterparts.[1–8] Among these anisotropic structures, anisotropic silver nanoplatelet/nanosheet has gained considerable attentions in recent years as a result of its fascinating plasmonic properties, biological activity, and long-term stability.[9] To date, a variety of solution-based conventional batch strategies have been developed to synthesize silver nanoplatelet/nanosheet, such as electrochemical synthesis, sonochemical route, biological synthesis, thermal synthesis, templating method, and chemical reduction.[10–16] However, most of these strategies generally require several hours or days for the nucleation and formation of silver nanoplatelet/nanosheet. In addition, precise control of the nucleation stage during the synthesis is still a great challenge facing these conventional batch strategies, which limit large scale production of anisotropic nanosized particles with consistent uniformity.[17] Therefore, the development of continuous, fast, and scalable process for the controllable synthesis of anisotropic silver nanostructures is still highly desirable for emerging fundamental and industrial applications.

Microfluidic microreactor technology represents a new frontier in the rational design and controllable synthesis of functional micro-/nanomaterials.[18–21] Microfluidics-enabled chemical engineering strategies rely on hydrodynamically confined micro/nanoliter volumes of reagents to interact with each other at the short-range millimeter-length or smaller scale. These unique characters endow microreactors many appealing features that conventional batch reactors can hardly achieve. For example, the large surface-to-volume ratio of microchannels allows highly efficient mass and heat transfer; fast reaction kinetics inside the microchannels within relatively short distances permits rapid particle production and the screening of experimental parameters; intensive mixing performance inside the microchannels increases the production yields; confining potentially toxic, explosive, and flammable starting reagents into a small space offers great possibilities to generate new materials; fully automatic operations enable greatly reduced local variations and easy scale-out. Therefore, microreactor may act as a promising platform for continuous, fast, and scalable synthesis of hierarchical anisotropic plasmonic nanostructures (e.g. $Ag@SiO_2$), which, to the best of our knowledge, have still not been reported yet.

This study presents a general and straightforward microfluidic strategy for continuous and ultrafast synthesis of hierarchical anisotropic plasmonic nanomaterials. Miniaturized spiral-shaped microreactor with two inlet flows, one containing $AgNO_3$, trisodium citrate (TSC), and H_2O_2 and the other $NaBH_4$, was employed to produce triangular silver (tAg) nanoplatelet. Hierarchical anisotropic silver core-silica shell ($Ag@SiO_2$) nanoparticles with tunable silica shell thickness were then successfully synthesized using the same two inlet flows microreactor of which one inlet contains tAg and tetraethyl orthosilicate (TEOS) and the other ammonia. The effect of a series of reaction conditions on the structural changes was examined. The cellular internalization difference of triangular nanoplatelets and their spherical counterparts by two different cancer cell lines (PANC-1 and MCF-7 cells) was further investigated.

2. Experimental details

2.1 Materials and reagents

Silver nitrate ($AgNO_3$), Tetraethyl orthosilicate (TEOS), Trisodium citrate (TSC), Hydrogen peroxide (H_2O_2, 30%), Sodium borohydride ($NaBH_4$), Ammonium hydroxide (25%), ethanol (200-proof), Fluorescein isothiocyanate (FITC), 3-Aminopropyltriethoxysilane (APTES), Hoechst 33342, Cell-counting kit-8 (CCK-8), were purchased from Sigma-Aldrich. Polydimethylsiloxane (PDMS Sylgard 184) was purchased from Dow Corning. Water used was from a Milli-Q water ultrapure water purification system. All chemicals were used as received without any further purification.

2.2 Fabrication of spiral-shaped microfluidic reactor for silver nanoplatelet synthesis

The two-loop microfluidic spiral channel with two inlets and one outlet was fabricated using standard photolithography and soft lithography. Briefly, film mask was designed with CAD software and ordered from Fine Line Imaging, Inc. The SU-8 mold was made by spin coating ca. 100 μm of SU-8 2035 photoresist onto a clean silicon wafer. Then, the PDMS precursor was poured over the master mold, left to solidify at 65 °C for 1 hour and peeled off to get the replica. Microchannels were formed by bonding the oxygen plasma treated PDMS replica to the glass slide.

2.3 Microfluidic synthesis of tAg

The synthesis of tAg was realized by simply using $AgNO_3$ (1 mM in water), TSC (7.5 mM in water), and H_2O_2 (100 mM in water) and the other $NaBH_4$ (3 mM in water). The two inlet flows were then pumped (Pump 33 DDS, Harvard Apparatus) into the spiral microchannel both at a flow rate of 0.5 mL/min to produce tAg. Afterward, the blue-colored solution was collected from the outlet.

2.4 Microfluidic synthesis of tAg@SiO_2

The synthesis of tAg@SiO_2 was realized using tAg (5 mM in ethanol) and TEOS (90 mM in ethanol) as one inlet and ammonia (1 M in ethanol) as the other inlet. The two inlet flows were then pumped into the microreactor at a flow rate of 50 and 100 μL/min, respectively, at room temperature. Afterward, the blue-whitish product was collected from the outlet.

2.5 COMSOL simulation and theoretical analysis for tAg and tAg@SiO_2 analysis

Firstly, Reynolds number (Re) was calculated to determine if the fluids are in laminar flow regimes: $Re = \rho UL/\mu$, where the density (ρ ~1000 kg/m^3) and dynamic viscosity (μ ~0.001 Pa·s) of water are used for approximations, L is the characteristic length, and U is the average flow velocity, which could be obtained by: $U = \frac{flow\ rate}{W \cdot H}$. In our case with the spiral microchannel, W = 500 μm, H = 50 μm, when flow rate is at 500 μL/min, U = 0.33 m/s, and Re = 7.58 < ~2300. When the flow rate of 100 μL/min or less is used in the synthesis of core-shell structure, the Re will be even smaller.

Therefore, the fluids are in laminar flow. We consider them as incompressible with no-slip boundary condition and neglect the gravity force for simplicity. The flow rates for two inlets

are set as 500 and 500 μL/min for tAg, and 50 and 100 μL/min for tAg@SiO2. The outlet is set to be fixed pressure with $p = 0$. The diffusion coefficient used is $D = 5 \times 10^{-10} m^2/s$, which is the value normally used for the mixing of water and ethanol.

2.6 Calculation of the synthesis time of tAg and tAg@SiO_2 via microfluidic device

In this study, the width and height of the microchannel are 500 and 50 μm, respectively. The spiral-shaped microchannel is made of three arcs with the diameters of 7.69 mm, 13.8 mm, and 22.2 mm, with the central angles of 180°, 180°, and 225°, respectively. To estimate the time for synthesis, firstly, the length of the channel is calculated, which is 7.73 cm. Then the volume of fluids in the channel is calculated to be 1.93 μL. Thus, with a flow rate of 500 μL/min, the time for the synthesis of tAg is ~0.23 s; Similarly, the time for the synthesis of tAg@SiO_2 is ~1.15 s.

2.7 Cellular culture and maintenance

PANC-1 (human pancreatic adenocarcinoma cell line) and MCF-7 (human breast adenocarcinoma cell line) cells were maintained in high glucose DMEM (Dulbecco's Modified Eagle's Medium, ATCC) supplemented with 10% FBS (ATCC) and 1% penicillin-streptomycin (Sigma) in a humidified incubator at 37 °C with 5% CO_2 and 95% air.

2.8 In vitro cytotoxicity evaluation

The cytotoxicity of sAg, sAg@SiO_2, tAg, and tAg@SiO_2 was evaluated using the CCK-8 viability assay. For the cytotoxicity evaluation, PANC-1 and MCF-7 cells were seeded at a density of 5000 cells per well in 96-well plates. After incubating the cells with sAg, sAg@SiO_2, tAg, and tAg@SiO_2 at a particle concentration ranging from 1 to 200 μg/mL for 24 h, 10 μL CCK-8 reagent was added to each well and incubated for 4 h. The absorbance of the resulting solution in each well was recorded at 450 nm with a microplate reader (TECAN SPARK 10M). Before reading, the plate was gently shaken on an orbital shaker for 30 s to ensure homogeneous distribution of color.

2.9 Conjugation of FITC onto core-shell nanoparticle surface

To conjugate FITC onto the surface of tAg@SiO_2 and sAg@SiO_2, firstly, APTES-FITC was prepared by stirring FITC in the mixed solution of ethanol (2 mL) and APTES (2 mL, the amount of FITC was 5 mol% of APTES) for 48 h under dark conditions. Then 50 μL of above solution was mixed with tAg@SiO_2 or sAg@SiO_2 (25 μg/mL, 20 mL) and then stirred for another 48 h under dark conditions. The solid product was obtained after centrifugation and finally dispersed into PBS for further analysis. The similar fluorescent intensity of the resultant tAg@SiO_2 and sAg@SiO_2 was confirmed with fluorescent spectroscopy for the following fluorescent tests.

2.10 Fluorescent measurement of the cellular internalization efficiency of tAg@SiO_2 and sAg@SiO_2

The procedures of cell culture, FITC conjugation, and cytotoxicity evaluation were described in the Supporting Information. For the qualitative investigation, PANC-1 and MCF-7 cells (10^5 per well) were separately seeded in a 6-well plate containing cover glasses

and were allowed to adhere for 24 h. After incubated with FITC-conjugated $tAg@SiO_2$ and $sAg@SiO_2$ (100 μg/mL) for 3 h, the cover glasses containing PANC-1 and MCF-7 cells were stained with Hoechst 33342 (10 μg/mL, 15 min) and then mounted onto glass slides. The slides were examined under a fluorescence microscope (Olympus BX51). For quantitative measurement, the cells were treated the same as above and then harvested by trypsinization. After the cells were collected, at least ten thousand of cells were acquired in FITC channel by flow cytometry (MACSQuant® Analyzer) and then analyzed by FlowJo software.

2.11 Characterization

Transmission electron microscopy (TEM) was performed on a Tecnai F20ST field emission gun (FEG) transmission electron microscope operating at an accelerating voltage of 200 kV. The energy-dispersive X-ray spectroscopic (EDS) measurements were performed with the spectrometer attached on the Tecnai F20ST FEG electron microscope.

3. Results and discussion

Microfluidic flow and continuous synthesis of triangular silver (tAg) nanoplatelet and silver core-silica shell ($tAg@SiO_2$) was carried out in the two-loop spiral-shaped microreactor with two inlets and one outlet (Figure 1). The height and the width of the microchannels are 50 and 500 μm, respectively. Three arcs with the diameters of 7.69, 13.8, and 22.2 mm (the central angles are 180°, 180°, and 225°, respectively) form the spiral-shaped microchannel with a total length of ca. 77 mm (Figure 2A). Given the unique merits of microfluidics, such a short range two-loop spiral-shaped microreactor is expected to synthesize desired anisotropic silver nanostructures in a continuous and ultrafast way. To demonstrate the possibility of the synthesis of tAg, the two inlet flows, one containing $AgNO_3$ (1 mM), TSC (7.5 mM), and H_2O_2 (100 mM) and the other $NaBH_4$ (3 mM), were pumped (Pump 33 DDS, Harvard Apparatus) into the microreactor both at a flow rate of 0.5 mL/min at room temperature (Figure 2A). The blue-colored reaction solution was collected from the outlet, and then the structures of the product were checked under transmission electron microscope (TEM). As revealed by the COMSOL simulation analysis (Figure 2B), complete and efficient mixing performance could be realized in such a short range two-loop spiral-shaped laminar flow microreactor due to the presence of special transverse Dean flow.[22–25] Observations from TEM images (Figures 2C&D) showed that well-defined triangular silver platelets having an average side length of ca. 80 nm and an average thickness of ca. 10 nm can be successfully fabricated in a large scale. This regular anisotropic nanoplatelet structure (Figure 2E) was confirmed by the top-view (Figure 2F) and the side-view (Figure 2G) of high resolution TEM images. Compared with the previous hour-/day-scale synthesis of silver nanoparticles,[26] it is also noteworthy that the synthesis of tAg from the microreactor only takes less than 250 ms (see calculation details in SI), revealing the ultrafast reaction kinetics from the microreactor, which is in accordance with the simulation analysis (Figure 2B). These results further demonstrated that such automatic microfluidic operation system could be employed as a promising platform for continuous, ultrafast, and scalable synthesis of anisotropic nanomaterials.

To explore the formation mechanism of tAg, we changed the concentrations of $AgNO_3$, TSC, H_2O_2, and $NaBH_4$ from the inlet flows and the flow rates of silver precursor fluid containing $AgNO_3$, TSC, and H_2O_2 (Figure 3). Since only one parameter was changed while the others were kept constant, the specific roles of each reagent in the synthesis of tAg were rationally investigated by examining the morphology changes of the silver products. Increasing the concentration of $AgNO_3$ (3 mM), the as-obtained product was a mixture of spherical nanoparticles and triangular nanoplatelets with a nanoplatelet yield of ca. 20% (Figure 3A). Decreasing the concentration of $AgNO_3$ (0.3 mM), silver nanoplatelet with high yield was obtained (Figure 3B). These findings indicated that a sufficient amount of oxidant in the system is needed to ensure that the silver is in the cationic form before reduction occurs.[17] If continuously increasing the concentrations of TSC (22.5 mM) or H_2O_2 (300 mM) from the inlet flows, well-defined triangular nanoplatelets were still formed (Figures 3C&E). However, only nearly spherical nanoparticles were obtained in the absence of TSC and H_2O_2 (Figures 3D&F). As revealed in the previous literature,[9,14,17] TSC is required to stabilize the formed silver nanoplatelet nuclei through preferential binding to the (111) faces, and H_2O_2 as an oxidative etchant is an essential component for helping to induce the formation of planar twinned seeds. Therefore, these findings confirmed that the presence of TSC and H_2O_2 could facilitate the formation of anisotropic nanoplatelets. Comparatively, changing the concentrations of $NaBH_4$ from the inlet flow, no matter increasing (9 mM) or decreasing (1 mM), only irregular-shaped nanoparticles were produced (Figures 3G&H), revealing the important roles of $NaBH_4$ as both reducing agent and capping agent in the regulation of the initiation time required for nanoplatelet nucleation.[17] In addition, changing the flow rates of silver precursor fluid obtained similar silver products as in the case of changing the concentrations of $AgNO_3$, *i.e.*, increasing the flow rates (2 mL/min) produced a mixture of spheres and nanoplatelets while decreasing the flow rates (0.1 mL/min) produced triangular nanoplatelets with a high yield (Figures 3I&J). These results not only revealed the key roles of TSC and H_2O_2 in the formation of anisotropic nanoplatelet but also confirmed that tAg can be obtained with high yield and great uniformity from microreactors when the reagents were added with an appropriate ratio into the inlet flows as well as a proper operation flow rates.

To improve the stability and biocompatibility of silver nanoplatelets,[27–29] microfluidics-enabled surface coating strategy was developed to synthesize hierarchical anisotropic silver core-silica shell nanostructures using the same short range two-loop spiral-shaped microreactor. The two inlet flows, one containing the as-synthesized tAg (5 mM) together with TEOS (90 mM) and the other ammonia (1 M), were pumped into the microreactor at a flow rate of 50 and 100 μL/min, respectively, at room temperature (Figure 4A). The blue-whitish product was collected from the outlet. The intensive mixing of tAg and silica precursor inside the two-loop microchannel, as revealed by the COMSOL simulation analysis (Figure 4B), permits the effective coating of silica on silver nanoplatelet surface. As shown in Figures 4C, core-shell structure can be successfully obtained in a large scale within 1.2 s. The presence of silica coating on the tAg surface was further confirmed by the EDX (Figure 4D), and the recognizable nanoplatelet morphology still remained (Figures 4C-F). Top-view and side-view of single silver core-silica shell tAg@SiO_2 particle in Figure 4G and Figure 4H, respectively, further confirmed a relatively uniform coating layer on tAg

surface with an average thickness of ca. 10 nm. These results, to the best of our knowledge, first demonstrated the feasibility of microreactors in the synthesis of hierarchical anisotropic plasmonic nanostructures.

To further investigate the tunability of such microreactor in the controllable synthesis of hierarchical silica-coated silver nanoparticles (AgNP@SiO_2, Figure 5A), we examined the effect of the flow rate on the morphology change of nanocomposite. As shown in Figure 5B, the thickness of silica shell can be well tuned from ca. 2 to 70 nm by changing the flow rates of ammonia fluid. The higher the flow rate of the ammonia, the thicker the coating layer of silica shell. Using the same microfluidic operation system, nearly spherical silver core-silica shell (sAg@SiO_2) having a coating layer of ca. 10 nm can be also successfully synthesized with one inlet flow containing spherical silver nanoparticles (sAg, from Figure 3D) and TEOS and the other ammonia (Figure 5C). These results not only confirmed the facile and effective features of microreactors in the controllable synthesis of anisotropic nanomaterials, but also indicated that microreactors could act as a general platform for constructing hierarchical core-shell nanostructures.

To examine the difference of the cellular activities between triangular and spherical silver nanomaterials, PANC-1 (human pancreatic adenocarcinoma cell line) and MCF-7 (human breast adenocarcinoma cell line) cells were employed to study the cell–particle interactions. As shown in Figure 6A, cytotoxicity test on PANC-1 cells showed that both tAg and sAg have a strong inhibiting effect on cancer cell growth due to the fast release of Ag^+ ions, but the half inhibitory concentration (IC_{50}) of sAg is 13 times higher than that of tAg, indicating the obvious shape-dependent anticancer activity of nanoparticles.[30] Similarly, the IC_{50} values of tAg and sAg toward MCF-7 cells are 11.2 and 110.5 μg/mL (Figure 6B), which further revealed the superior advantage of anisotropic nanostructures as cancer theranostics.[30] It is also noted that the silica coating endows both tAg@SiO_2 and sAg@SiO_2 with significantly improved biocompatibility, no obvious cytotoxicity on PANC-1 and MCF-7 cells was observed with particle concentrations up to 200 μg/mL (Figures 6A&B). This can be attributed to the significantly reduced release rate of Ag^+ ions by the silica coating layer, which limits the accessibilities of silver ions to cells.[31]

To explore the in-depth cell–particle interactions, we conjugated FITC on the particle surface of tAg@SiO_2 and sAg@SiO_2 and compared their cellular internalization efficiency. Fluorescent microscopy and flow cytometry were used to qualitatively and quantitatively measure the fluorescence intensity of cells, respectively. As shown in Figure 7A, fluorescent microscopy results clearly demonstrated that the tAg@SiO_2-treated cells show brighter green fluorescence than sAg@SiO_2-treated cells, for both PANC-1 and MCF-7 cell lines, when acquired at the same exposure time. In addition to the particle shape-dependent cellular internalization, cell type also plays important roles where PANC-1 cells exhibited higher cellular fluorescent intensity than MCF-7 cells after treated by both kinds of nanoparticles. These results were further confirmed by the flow cytometry analysis that the mean fluorescence intensity (MFI) values of tAg@SiO_2-treated PANC-1 and MCF-7 cells are 5.9 and 7.1 times higher than those of sAg@SiO_2-treated ones, respectively (Figures 7B&C), showing the obviously enhanced cellular internalization from the anisotropic nanostructures in comparison with their spherical counterparts. This is probably caused by

the relatively fast cytomembrane wrapping time and/or a more favorable endocytosis pathway of nonspherical particles.[32–34] These results shed new lights on the particle shape-dependent cellular behavior, which may provide important guidelines for the custom design of novel materials for application in nanomedicines.

4. Conclusions

In summary, we have reported a facile and straightforward microfluidic strategy for continuous and ultrafast synthesis of hierarchical anisotropic silver nanomaterials using a short range two-loop spiral-shaped laminar flow microreactor. Triangular silver platelets can be produced within 250 ms in a large scale using one inlet flow containing $AgNO_3$, TSC, and H_2O_2 and the other $NaBH_4$. Both the reactant concentration and the flow rate were found to play important roles in the formation of nanoplatelet structures. Hierarchical anisotropic silver core-silica shell (tAg@SiO_2) with tunable silica shell thickness was then successfully synthesized at the seconds scale in the same two inlet microreactor with one containing tAg and TEOS and the other ammonia. The IC_{50} values of tAg toward PANC-1 and MCF-7 cells were significantly lower than those of sAg. The obviously enhanced cellular internalization of triangular nanoplatelets by PANC-1 and MCF-7 cells was also investigated in comparison with their spherical counterparts. These findings not only bring new insights for engineering micro-/nanomaterials from microfluidic reactors but also provide important guidance for the rational design of functional optoelectronics and biomaterials.

ACKNOWLEDGMENT

This work was sponsored by the NIH Director's Transformative Research Award (R01HL137157), and NSF grants (ECCS 1128677, 1309686, 1509369). We gratefully acknowledge the support from the Electron Microscope Facility at Dartmouth College.

REFERENCES

[1]. Zheng NC, Wang Z, Long JY, Kong LJ, Chen DY, Liu ZQ, Shape-dependent adsorption of CeO2nanostructures for superior organic dye removal, J. Colloid Interf. Sci 525 (2018) 225–233. doi:10.1016/j.jcis.2018.03.087.

[2]. Rakshit S, Moulik SP, Bhattacharya SC, Understanding the effect of size and shape of gold nanomaterials on nanometal surface energy transfer, J. Colloid Interf. Sci 491 (2017) 349–357. doi:10.1016/j.jcis.2016.12.052.

[3]. Murphy RP, Hong K, Wagner NJ, Synthetic control of the size, shape, and polydispersity of anisotropic silica colloids, J. Colloid Interf. Sci 501 (2017) 45–53. doi:10.1016/j.jcis.2017.04.026.

[4]. Blanco E, Shen H, Ferrari M, Principles of nanoparticle design for overcoming biological barriers to drug delivery, Nat. Biotechnol 33 (2015) 941–951. doi:10.1038/nbt.3330. [PubMed: 26348965]

[5]. Zhang H, Jin M, Xiong Y, Lim B, Xia Y, Shape-Controlled Synthesis of Pd Nanocrystals and Their Catalytic Applications, Acc. Chem. Res 46 (2013) 1783–1794. doi:10.1021/ar300209w. [PubMed: 23163781]

[6]. Champion J a, Mitragotri S, Role of target geometry in phagocytosis., Proc. Natl. Acad. Sci. U.S.A 103 (2006) 4930–4934. doi:10.1073/pnas.0600997103. [PubMed: 16549762]

[7]. Geng Y, Dalhaimer P, Cai SS, Tsai R, Tewari M, Minko T, Discher DE, Shape effects of filaments versus spherical particles in flow and drug delivery, Nat. Nanotechnol 2 (2007) 249–255. doi: 10.1038/nnano.2007.70. [PubMed: 18654271]

[8]. Hao N, Li LF, Tang FQ, Roles of particle size, shape and surface chemistry of mesoporous silica nanomaterials on biological systems, Int. Mater. Rev 62 (2017) 57–77. doi: 10.1080/09506608.2016.1190118.

[9]. Wiley B, Sun Y, Mayers B, Xia Y, Shape-Controlled Synthesis of Metal Nanostructures: The Case of Silver, Chem. Eur. J 11 (2005) 454–463. doi:10.1002/chem.200400927. [PubMed: 15565727]

[10]. Métraux GS, Mirkin CA, Rapid Thermal Synthesis of Silver Nanoprisms with Chemically Tailorable Thickness, Adv. Mater 17 (2005) 412–415. doi:10.1002/adma.200401086.

[11]. Jin R, Charles Cao Y, Hao E, Métraux GS, Schatz GC, Mirkin CA, Controlling anisotropic nanoparticle growth through plasmon excitation, Nature. 425 (2003) 487–490. doi:10.1038/nature02020. [PubMed: 14523440]

[12]. Yang X, Yu Y, Gao Z, A highly sensitive plasmonic DNA assay based on triangular silver nanoprism etching, ACS Nano. 8 (2014) 4902–4907. doi:10.1021/nn5008786. [PubMed: 24766422]

[13]. Millstone JE, Hurst SJ, Métraux GS, Cutler JI, Mirkin CA, Colloidal Gold and Silver Triangular Nanoprisms, Small. 5 (2009) 646–664. doi:10.1002/smll.200801480. [PubMed: 19306458]

[14]. Kim MH, Yoon DK, Im SH, Growth pathways of silver nanoplates in kinetically controlled synthesis: Bimodal versus unimodal growth, RSC Adv. 5 (2015) 14266–14272. doi:10.1039/c4ra12818d.

[15]. Xu R, Xie T, Zhao Y, Li Y, Single-crystal metal nanoplatelets: Cobalt, nickel, copper, and silver, Cryst. Growth Des 7 (2007) 1904–1911. doi:10.1021/cg060593a.

[16]. Chen H, Simon F, Eychmüller A, Large-scale synthesis of micrometer-sized silver nanosheets, J. Phys. Chem. C 114 (2010) 4495–4501. doi:10.1021/jp909206x.

[17]. Zhang Q, Li N, Goebl J, Lu Z, Yin Y, A systematic study of the synthesis of silver nanoplates: Is citrate a “magic” reagent?, J. Am. Chem. Soc 133 (2011) 18931–18939. doi:10.1021/ja2080345. [PubMed: 21999679]

[18]. Il Park J, Saffari A, Kumar S, Günther A, Kumacheva E, Microfluidic Synthesis of Polymer and Inorganic Particulate Materials, Annu. Rev. Mater. Res 40 (2010) 415–443. doi:10.1146/annurev-matsci-070909-104514.

[19]. Marre S, Jensen KF, Synthesis of micro and nanostructures in microfluidic systems., Chem. Soc. Rev 39 (2010) 1183–1202. doi:10.1039/b821324k. [PubMed: 20179831]

[20]. Hao N, Nie Y, Zhang JXJ, Microfluidic synthesis of functional inorganic micro-/nanoparticles and applications in biomedical engineering, Int. Mater. Rev 63 (2018) 461–487. doi: 10.1080/09506608.2018.1434452.

[21]. Elvira KS, Casadevall i Solvas X, Wootton RCR, de Mello AJ, The past, present and potential for microfluidic reactor technology in chemical synthesis., Nat. Chem 5 (2013) 905–915. doi: 10.1038/nchem.1753. [PubMed: 24153367]

[22]. Hao N, Nie Y, Closson AB, Zhang JXJ, Microfluidic synthesis and on-chip enrichment application of two-dimensional hollow sandwich-like mesoporous silica nanosheet with water ripple-like surface, J. Colloid Interf. Sci 539 (2019) 87–94. doi:10.1016/j.jcis.2018.12.040.

[23]. Di Carlo D, Inertial microfluidics., Lab Chip. 9 (2009) 3038–3046. doi:10.1039/b912547g. [PubMed: 19823716]

[24]. Hao N, Nie Y, Shen T, Zhang JXJ, Microfluidics-enabled rational design of immunomagnetic nanomaterials and their shape effect on liquid biopsy, Lab Chip. 18 (2018) 1997–2002. doi: 10.1039/C8LC00273H. [PubMed: 29923569]

[25]. Hao N, Nie Y, Zhang JXJ, Microfluidic Flow Synthesis of Functional Mesoporous Silica Nanofibers with Tunable Aspect Ratios, ACS Sustain. Chem. Eng 6 (2018) 1522–1526. doi: 10.1021/acssuschemeng.7b03527.

[26]. Rycenga M, Cobley CM, Zeng J, Li W, Moran CH, Zhang Q, Qin D, Xia Y, Controlling the synthesis and assembly of silver nanostructures for plasmonic applications, Chem. Rev 111 (2011) 3669–3712. doi:10.1021/cr100275d. [PubMed: 21395318]

[27]. Meleppat RK, Prabhathan P, Keey SL, Matham MV, Plasmon resonant silica-coated silver nanoplates as contrast agents for optical coherence tomography, J. Biomed. Nanotechnol 12 (2016) 1929–1937. doi:10.1166/jbn.2016.2297. [PubMed: 29360336]

[28]. Brandon MP, Ledwith DM, Kelly JM, Preparation of saline-stable, silica-coated triangular silver nanoplates of use for optical sensing, J. Colloid Interf. Sci 415 (2014) 77–84. doi:10.1016/j.jcis.2013.10.017.

[29]. Thomas R, Phua SZF, Sreejith S, Zhao Y, Soh CB, Light intensity field enhancement (LIFE) induced localized edge abrasion of silica-coated silver nanoprisms, Nanoscale. 9 (2017) 15356–15361. doi:10.1039/c7nr03171h. [PubMed: 28831487]

[30]. Hao N, Li L, Tang F, Shape matters when engineering mesoporous silica-based nanomedicines, Biomater. Sci 4 (2016) 575–591. doi:10.1039/C5BM00589B. [PubMed: 26818852]

[31]. Sousa FL, Almeida A, Girão AV, Fateixa S, Trindade T, Multiple emulsion templating of hybrid Ag/SiO2 capsules for antibacterial applications, Part. Part. Syst. Char 32 (2015) 561–566. doi:10.1002/ppsc.201400168.

[32]. Hao N, Li L, Zhang Q, Huang X, Meng X, Zhang Y, Chen D, Tang F, Li L, The shape effect of PEGylated mesoporous silica nanoparticles on cellular uptake pathway in Hela cells, Microporous Mesoporous Mater. 162 (2012) 14–23. doi:10.1016/j.micromeso.2012.05.040.

[33]. Hao N, Nie Y, Tadimety A, Shen T, Zhang JXJ, Microfluidics-enabled rapid manufacturing of hierarchical silica-magnetic microflower toward enhanced circulating tumor cell screening, Biomater. Sci 6 (2018) 3121–3125. doi:10.1039/C8BM00851E. [PubMed: 30375583]

[34]. Huang XL, Teng X, Chen D, Tang FQ, He JQ, The effect of the shape of mesoporous silica nanoparticles on cellular uptake and cell function., Biomaterials. 31 (2010) 438–448. doi:10.1016/j.biomaterials.2009.09.060. [PubMed: 19800115]

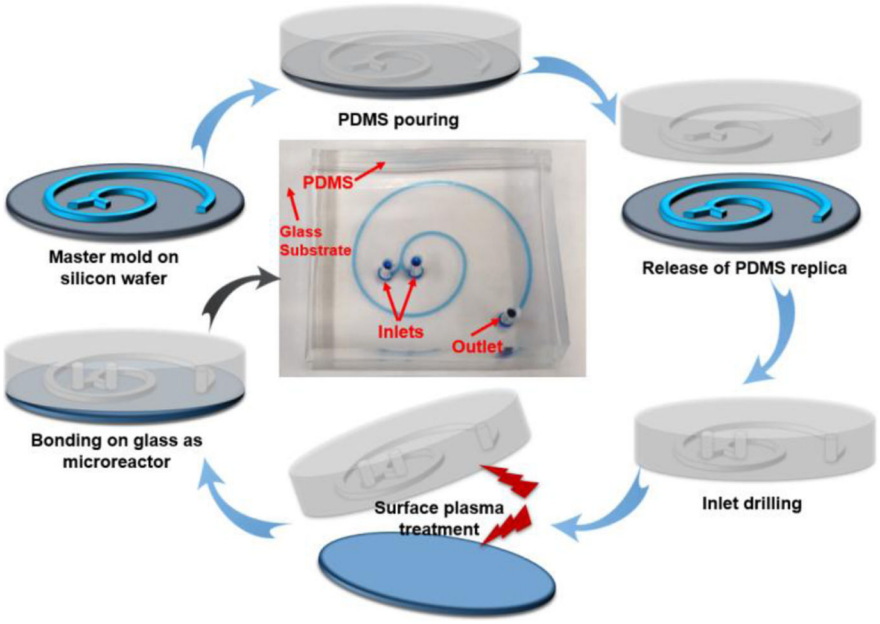

Figure 1.

Fabrication procedure of 2-loop spiral-shaped microfluidic device. The central image is a photograph of the fabricated two-run microreactor. The microfluidic channel was filled with a blue dye for visualization.

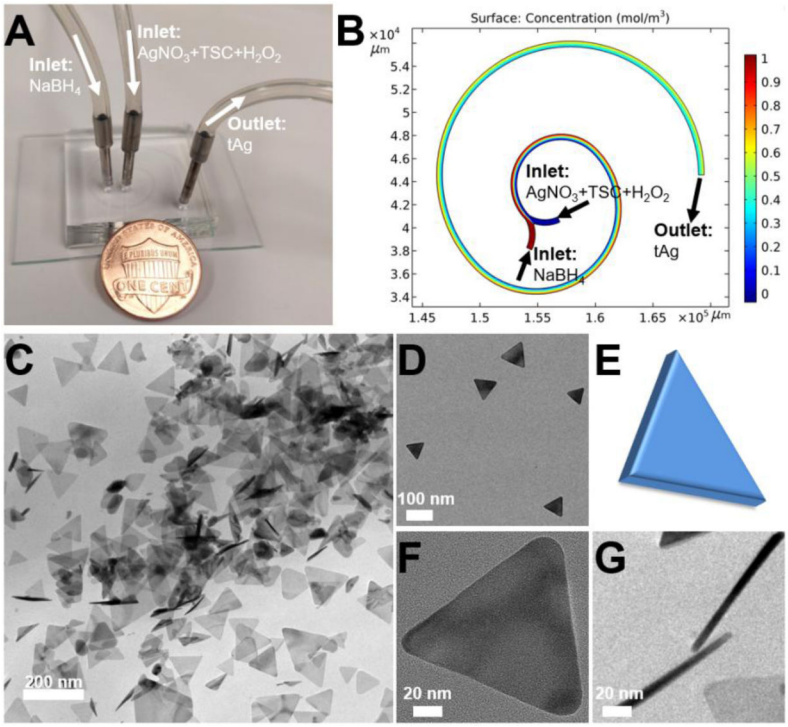

Figure 2.

Microfluidic synthesis of triangular silver (tAg) nanoplatelet. (A) Experimental setup for the synthesis of tAg, with a U.S. one cent coin for scale. (B) Simulation result of mixing in two-loop spiral-shaped microchannel. (C,D) TEM images of tAg at different magnifications. (E) Schematic drawing of the structure of tAg. (F) and (G) are the top-view and side-view of tAg, respectively.

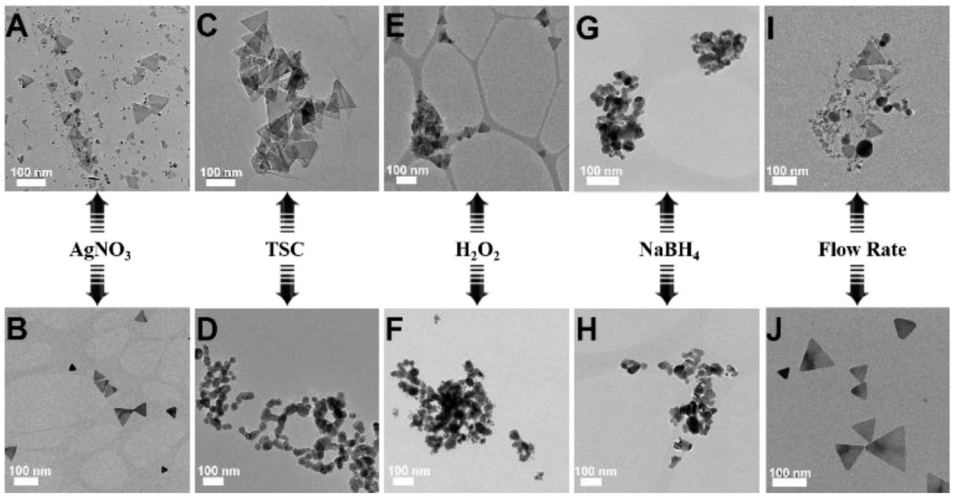

Figure 3.

Effect of a series of reaction parameters, including the concentration of $AgNO_3$ (A,B), the concentration of TSC (C,D), the concentration of H_2O_2 (E,F), the concentration of $NaBH_4$ (G,H), and the flow rate of silver precursor fluid (I,J), on the structural changes of silver nanoparticles.

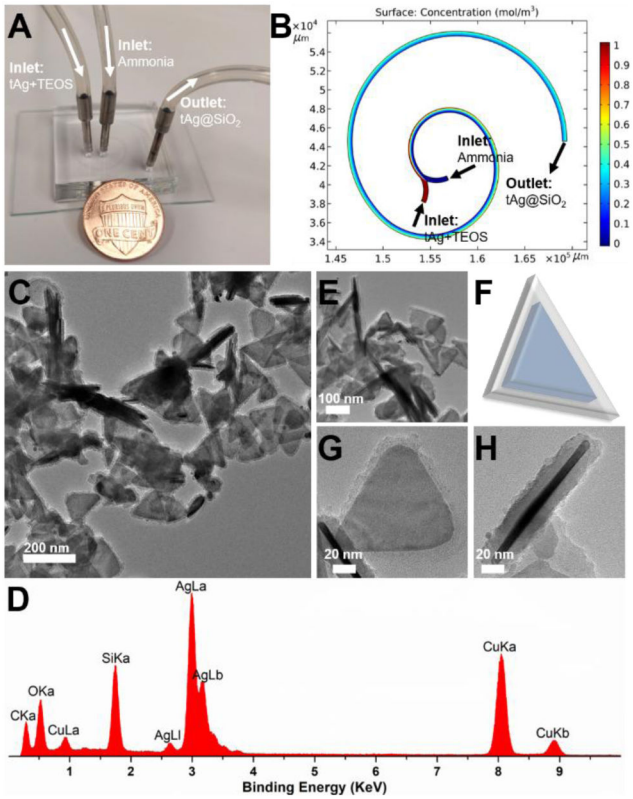

Figure 4.

Microfluidic synthesis of triangular core-shell $tAg@SiO_2$. (A) Experimental setup for the synthesis of $tAg@SiO_2$, with a U.S. one cent coin for scale. (B) Simulation result of mixing in two-loop spiral-shaped microchannel. (C,E) TEM images of $tAg@SiO_2$ at different magnifications. (D) $tAg@SiO_2$(F) Schematic drawing of the structure of $tAg@SiO_2$. (G) and (H) are the top-view and side-view of $tAg@SiO_2$, respectively.

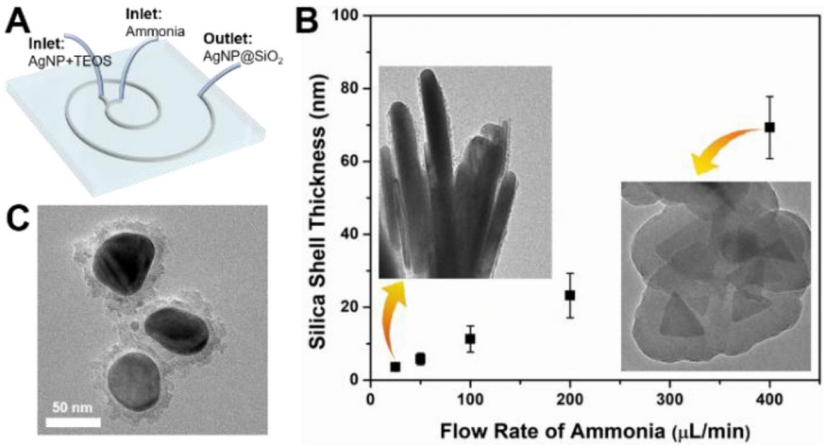

Figure 5.

Microfluidics-mediated general platform for the flow synthesis of silica-coated silver nanoparticles (AgNP@SiO_2). (A) Schematic drawing to show the formation of core-shell AgNP@SiO2. (B) The thickness control of the silica shell by varying the flow rate of ammonia, the insets are two TEM images showing the silica coating on silver nanoplatelets. (C) TEM image of spherical core-shell nanocomposite formed by the same two-run microreactor.

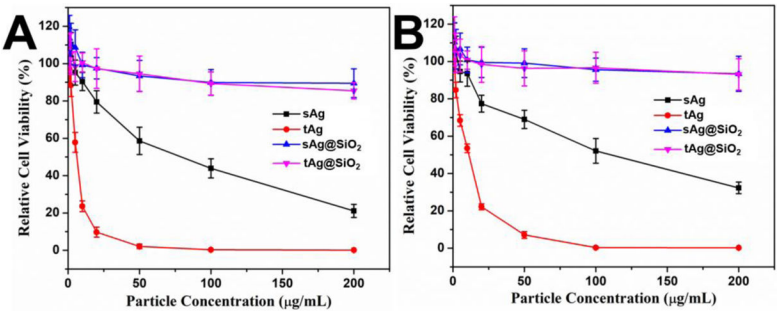

Figure 6.

Comparison of cellular viability between the triangular and the spherical silver nanomaterials. (A) and (B) are PANC-1 and MCF-7 cell viability with particle concentrations of sAg, tAg, sAg@SiO_2, and tAg@SiO_2 from 1 to 200 μg/mL for 24 hours, respectively.

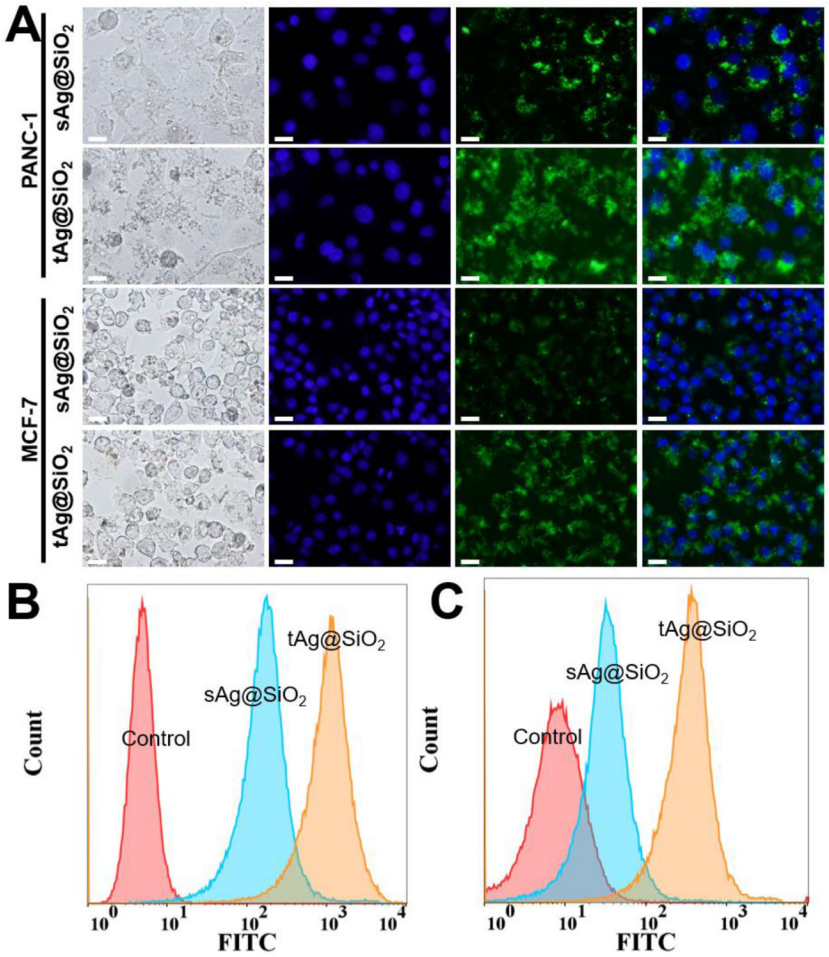

Figure 7.

Comparison of cellular internalization efficiency between the triangular and the spherical silver nanomaterials. (A) Bright-field and fluorescence images of PANC-1 and MCF-7 cells treated by $sAg@SiO_2$ and $tAg@SiO_2$ with a particle concentration of 100 μg/mL for 3 hours. The blue and green colors came from Hoechst 33342 and FITC-labeled nanoparticles. All scale bars denote a length of 20 μm. (B) and (C) are the flow cytometry analysis of core-shell nanoparticles-treated PANC-1 and MCF-7 cells, respectively.